Regular Article

PHYSICAL CHEMISTRY RESEARCH
Published by the
Iranian Chemical Society
www.physchemres.org
info@physchemres.org

*Phys. Chem. Res., Vol. 12, No. 4, 881-899, December 2024*
**DOI: 10.22036/pcr.2024.440352.2472**

# Explanation of the Quinoxaline Analog's Adsorption and Inhibition Mechanism for Carbon Steel Corrosion in 1 M HCl Based on Experiments and Theoretical Calculations

L. Chahir[a], M. El Faydy[b,*], L. Adlani[c], N. Abad[d], I. Warad[e,f], F. Benhiba[a,g], D. Benmessaoud Left[h], M. Zertoubi[h], M. Allali[i], B. Dikici[j], G. Kaichouh[a], Y. Ramli[d,k] and A. Zarrouk[a,f,*]

[a]*Laboratory of Materials, Nanotechnology and Environment, Faculty of Sciences, Mohammed V University in Rabat, P. O. Box: 1014, Rabat, Morocco*

[b]*Laboratory of Organic Chemistry, Inorganic, Electrochemistry, and Environment, Department of Chemistry, Faculty of Sciences, Ibn Tofaïl University, P. O. Box: 133, 14000, Kenitra, Morocco*

[c]*Laboratory of Advanced Materials and Process Engineering, Faculty of Sciences, Ibn Tofail University, P. O. Box: 133, 14000, Kenitra, Morocco*

[d]*Laboratory of Medicinal Chemistry, Drug Sciences Research Center, Faculty of Medicine and Pharmacy, Mohammed V University, Rabat, Morocco*

[e]*Department of Chemistry, AN-Najah National University, P. O. Box: 7, Nablus, Palestine*

[f]*Research Centre, Manchester Salt & Catalysis, Unit C, 88-90 Chorlton Rd, M15 4AN, Manchester, United Kingdom*

[g]*Higher Institute of Nursing Professions and Health Techniques of Agadir Annex Guelmim, Morocco*

[h]*Laboratory of Interface Materials Environment, Faculty of Sciences Aïn Chock, Hassan II University of Casablanca BP, 5366, Morocco*

[i]*Institute of Nursing Professions and Health Techniques Fez, EL Ghassani Hospital, Fez 30000, Morocco*

[j]*Ataturk University, Department of Mechanical Engineering, 25240 Erzurum, Erzurum, Turkey*

[k]*Mohammed VI Center for Research and Innovation (CM6), Rabat 10000, Morocco*

*(Received 28 January 2024, Accepted 15 June 2024)*

In this work, we tested the effectiveness of phenyl-1-propyl quinoxaline-2(1H)-one (PRQX), a novel quinoxaline analog, as a corrosion inhibitor for carbon steel (C-S) in a 1 M HCl electrolyte. Incorporating numerous techniques, such as scanning electron microscopy (SEM), electrochemical impedance spectroscopy (EIS), energy dispersive X-ray spectroscopy (EDX), and UV-visible spectroscopy, we examined the inhibitory properties of PRQX. PRQX maximum anti-corrosion efficiency was determined to be 97.7% at $10^{-3}$ M dose at 303 K temperature. PRQX displayed a mixed-type inhibitor effect, slowing anodic and cathodic corrosion processes, as indicated by PPD tests. The PRQX molecule binds to the C-S surface in compatibility with the Langmuir adsorption model. UV-visible analysis of the inhibited electrolyte clearly reveals the complexation of the $Fe^{2+}$ with the PRQX molecule. Additionally, using density functional theory (DFT) and molecular dynamics simulation (MDS), conceptual analysis of the PRQX molecule's most reactive sites and its adsorption process were carried out.

**Keywords:** Quinoxaline analog, Corrosion inhibitor, PDP/EIS, SEM/EDX, DFT/MDS

## INTRODUCTION

During service, metal materials are degraded by the influences of bordering corrosive environments, which is known as the corrosion of metals. Large-scale economic losses and resource waste have been brought on by metal corrosion [1,2]. In addition, it poses significant security dangers and might endanger human life. As a consequence, research on metal corrosion resistance has always been a hot

*Corresponding authors. E-mail: mohamed.elfaydy@gmail.com; azarrouk@gmail.com

topic for scientists [3].

Carbon steel is employed most primarily as a material for building and construction and extensively applied in the industrial field due to its connection with a multitude of advantages, including strong mechanical power and cost-effectiveness. When carbon steel is treated to the acid pickling and cleaning process, the fundamental issue is that it corrodes easily, resulting in significant economic and industrial losses [4,5]. As a result, the corrosion resistance of C-S is extremely significant. Since its ease of use, low cost, and impressive results make the inhibitor one of the numerous corrosion protection techniques that are important to utilize [6,7].

Generally, organic substances form a protective barrier at the metal/environment interface to limit corrosion [8-18]. According to a review of the scientific literature, the majority of heterocyclic and aromatic compounds that contain heteroatoms like sulfur, nitrogen, and oxygen, as well as π-electrons and functional groups, successfully prevent steel corrosion by binding to the active donor-receptor sites found in the inhibitor's molecular structure [19-22].

Quinoxalines are heterocyclic compounds with N and O atoms that are biologically active and employed in diverse antibiotics [23-26]. Aside from biological features, some quinoxaline compounds exhibit remarkable properties in the field of metal anti-corrosion. Recently, certain investigations in science on quinoxaline derivatives as corrosion inhibitors have been published. For example, Lukman O. Olasunkanmi and al. [27]. researched the anti-corrosion nature of 1-[3-(3-methoxyphenyl)-5-(quinoxalin-6-yl)-4,5-dihydropyrazol-1-yl]propan-1-one (Mt-3-PQPP) and 1-(3-(4-chlorophenyl)-5-(quinoxalin-6-yl)-4,5-dihydro-1H-pyrazol-1-yl)propan-1-one (Cl-4-PQPP) for mild steel in 1 M HCl. The PDP experimental findings suggest that the corrosion inhibition performances of Mt-3-PQPP and Cl-4-PQPP were found to be 90.28 and 89.82%, respectively, at 2.75 $10^{-4}$ M. The anti-corrosion abilities of 3-(4-(dimethylamino) quinoxalin-2(1H)-one (NSQN) and 3-(4-chlorostyryl) quinoxalin-2(1H)-one (CSQN) on mild steel in 1 M HCl have been examined by Laabaissi and al. [28] PDP data manifests that the anti-corrosion performances of CSQN and NSQN are close to 91.1 and 94.5%, respectively, at $10^{-3}$ M. Benhiba and al. [29] studied the corrosion inhibitory nature of (6-methyl-2-(p-tolyl)-1,4-dihydroquinoxaline ($(CH_3)_2Q$) for mild steel in 1 M HCl. The EIS information reveals that the anticorrosion performance of $(CH_3)_2Q$ can reach 94.3% at 0.001 M. Producing a highly effectiveness inhibitor remains challenging due to the wide range of chemical molecules along with other obstacles, notwithstanding major breakthroughs in inhibitor research.

In the present investigation, the newly synthesized quinoxalinone derivative inhibited the corrosion of C-S in 1 M HCl, 3-phenyl-1-propylquinoxalin-2(1H)-one (PRQX), was evaluated. This was done using EIS, PDP, weight loss, UV-visible spectroscopy, SEM, and EDX. As well, DFT and MDS were applied to validate the experimental findings.

## EXPERIMENTAL PROCEDURE

### Substrate and Electrolyte

The substrate to be worked on is carbon steel (C-S). Its chemical makeup is as follows (in weight percent): C:0.370; Si:0.230; Mn:0.680; S:0.016; Cr:0.077; Ti:0.011; Ni:0.059; Co:0.009; Cu:0.160, and the rest in iron (Fe). The dimensions of C-S substrates for weight loss and electrochemical tests were 1.5 × 1.5 × 0.3 ($cm^3$) and 1.0 $cm^2$, respectively. Prior to each use, the investigated C-S substrates were meticulously polished with emery paper ranging from 180 to 1200. Following polishing, the backing materials were dried, cleaned with distilled water, and dehydrated with acetone. All treatments of C-S substrates were made according to the standard methods [30].

The corrosive medium employed is a 1 M acidic electrolyte. This electrolyte was prepared by diluting a concentrated 37% HCl, analytical grade, with distilled water.

### Inhibitor

The availability of several nitrogen and oxygen atoms, its large size, many π-bonds (conjugated system), and its overall solubility in HCl were all factors in the selection of quinoxaline. Figure 1 shows the chemical structure of 3-phenyl-1-propylquinoxalin-2(1H)-one (PRQX). The concentrations of PRQX varied between $10^{-3}$ M and $10^{-6}$ M.

### Weight Loss Experiments

The C-S substrates were precisely weighed before being submerged for 6 h at 303 K in the acidic electrolyte that contains and does not contain PRQX varying doses of PRQX.

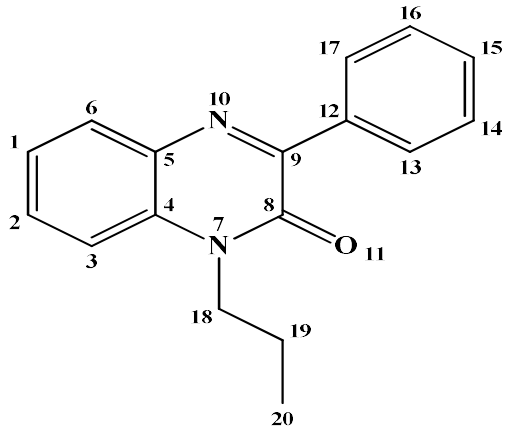


**Fig. 1.** Molecular structure of 3-phenyl-1-propylquinoxalin-2(1H)-one.

After being submerged in the acidic electrolyte, the substrates were collected, washed, dried, and precisely weighed. The corrosion rate ( $C_r$ ) in mg $cm^{-2}$ $h^{-1}$ and the effectiveness of the inhibition $\eta_{WL}(\%)$ were ascertained using the subsequent formulas [31]:

$$C_r = \frac{\Delta\omega}{S \times t} = \frac{\omega^b - \omega^a}{S \times t} \quad (1)$$

$$\eta_{WL}(\%) = \frac{C_r^\circ - C_r^{inh}}{C_r^\circ} \times 100 \quad (2)$$

where $\omega^b$ and $\omega^a$ stand for the substrate weights (mg) both prior to and post being submerged in various electrolytes, respectively. *S* is the exposed area ($cm^2$), *t* is the exposure time (h), $C_r^{inh}$ and $C_r^\circ$ represent the rates of unrestricted electrolyte corrosion when using and without PRQX, respectively.

## Electrochemical Experiments

All electrochemical tests were undertaken utilizing a temperature-controlled double-walled cylindrical glass cell. Three different electrodes and a PGZ 100 potentiostat were installed in the cell, and a computer running the Voltamaster 4 application was used to regulate them. In this new cell configuration, a saturated calomel reference electrode (SCE) was used, along with a platinum disc as the counter electrode, and a C-S electrode as the working electrode. All experiments were carried out at a constant temperature of 303 K. Before the start of each electrochemical investigation, for a 30-minute period, the C-S electrode was submerged in the electrolytes to provide a constant open circuit voltage ($E_{OCP}$). The measures of the EIS at the $E_{OCP}$ have been performed by employing a frequency range of $10^5$ Hz to $10^{-1}$ Hz with an amplitude of 10 mV. Further, PDP analyses were realized with a scan rate of $5.10^{-1}$ mV $s^{-1}$ across -0.8 V and -0.1 V. Relationships (3) and (4) are used to estimate the corrosion inhibitory efficacies resulting from EIS and PDP data, respectively [32]:

$$\eta_{EI}(\%) = \left(\frac{R_P - R_P^0}{R_P}\right) \times 100 = \frac{\theta}{100} \quad (3)$$

where $R_P^0$ and $R_P$ stand for the polarization resistances of unfettered electrolyte using and without PRQX, respectively.

$$\eta_{PP}(\%) = \left(\frac{i_0 - i}{i_0}\right) \times 100 \quad (4)$$

where, respectively, $i$ and $i_0$ indicate the densities of corrosion current in the absence and presence of PRQX.

## Surface Analysis

SEM-EDX analyses were performed on carbon steel substrates before and after 24 h of immersion in 1 M HCl in the presence and absence of the inhibitor molecule at 303 K using scanning electron microscopy. Since we have previously operated under similar working conditions and on the same type of material, we used the same information concerning the effects of concentration and temperature (assessment of inhibitor performance by gravimetry and electrochemical techniques), as well as the surface analysis results obtained during our work on carbon steel [33].

## UV-visible Analysis

To assess the probable formation of the iron-inhibitor complex when immersing C-S in the inhibited electrolytes. The 1 M HCl media containing $10^{-3}$ M of PRQX was analyzed pre and post-72h of C-S submerged employing a

Jenway (series 730) UV-visible spectrophotometer.

## DFT Information

Quantum chemical simulations are utilized to take a view at the electronic structure of organic compounds in the environment of corrosion [34]. The structure and charge properties of the inhibitor molecule have a considerable impact on how it adheres to the metal surface during corrosion inhibition [35]. We wanted to comprehend the mechanism by which PRQX acts on the C-S surface using the aqueous phase DFT approach [36]. Using this theoretical adjunction, it was likewise possible to relate the expected experiential inhibitory efficiency of neutral to the chemical reactivity indices [37,38]. The chemical quantum computation was conducted using Gaussian 09 W software with the DFT/B3LYP/6-311++G(d,p). The conceptual specifications of chemical reactivity, such as the energies of the most occupied molecular orbitals ("$E_{HOMO}$") and the least occupied molecular orbitals ("$E_{LUMO}$"), the energy gap ("ΔE"), the overall electronegativity ("χ"), the overall hardness ("η") and the electron transfer from the occupied orbitals of organic molecules to the unoccupied orbitals of a metal surface ("ΔN110"), were calculated. In the case of Fe(110), the theoretical value of "χ" is determined by the work function "Φ", with Φ = χ (Fe110) = 4.82 eV, and "η" represents the metallic mass (η (Fe110) = 0 eV) [39,40].

$$\Delta E = E_{LUMO} - E_{HOMO} \quad (5)$$

$$\chi = \frac{1}{2}\left(E_{HOMO} + E_{LUMO}\right) \quad (6)$$

$$\eta = \frac{1}{2}\left(E_{HOMO} - E_{LUMO}\right) \quad (7)$$

$$\Delta N_{110} = \frac{\chi_{Fe_{110}} - \chi_{inh}}{2\left(\eta_{Fe_{110}} + \eta_{inh}\right)} = \frac{\Phi - \chi_{inh}}{2\eta_{inh}} \quad (8)$$

## MDS Information

Due to its capacity to track the interatomic interactions between the two, the Molecular Dynamics Method (MDS) is especially well adapted to examining the adherence of an inhibitor substance to a metallic support [41]. The Materials Studio 2016 (MS 2016) program's Forcite module, which is integrated, was employed to carry out this simulation. The interactions for the tested system were achieved by means of a simulation box (27.30× 27.30 × 37.13 $Å^3$) with a 6-layer slab for the $Fe_{(110)}$ in each layer corresponding to a unit cell (11 × 11) and a vacuum spacing of 33 Å along the z-direction separating periodic image in each direction. In addition to the iron layer, the solvent layers were generated through an amorphous cell module, consisting of a PRQX molecule, 491 water molecules, and 9 each of $H_3O^+$ and $Cl^-$ ions. The Andersen thermostat was employed to keep the simulation system's temperature constant. This model is an NVT, which means that the temperature (T), the volume (V), and the number of particles (N) are all kept constant. For the duration of the simulation, which lasted $10^3$ ps (picoseconds) with a time step of 1 fs (femtosecond), the temperature was set at 303 K. The system's particle interactions were calculated using the COMPASS force domain [42].

# RESULTS AND DISCUSSIONS

## Weight Loss Investigation

An easy and most reliable way to evaluate the performance of inhibitors is by measuring weight loss (WL). The WL parameters of C-S in the unfettered electrolyte using and without PRQX at 303 K are shown in Table 1. Observably, with the inclusion of PRQX in the acidic electrolyte, the $C_r$ of C-S was considerably diminished, likely due to the good defense of the metallic surface. Additionally, the values of $\eta_{WL}(\%)$ raise with increasing amounts of PRQX, which is likely results from the adsorption of PRQX compound at the C-S area [43]. Specifically, when PRQX concentration was increased up to $10^{-3}$ M, the decrease in $C_r$ value became more pronounced, and the $\eta_{WL}(\%)$ value increased to reach a maximum of 95.2%. The presence of nitrogen and oxygen atoms in the PRQX chemical can function as adsorption sites and participate in molecular relationships with the vacated orbitals of the Fe atoms. Also, the large size of the PRQX molecule allows coverage of a large number of active centers. All this makes the PRQX work efficiently.

**Table 1.** Weight Loss Indices for C-S in Unfettered Electrolyte Using and without PRQX at 303 K

| Electrolyte | C (M) | $C_r$ (mg $cm^{-2}$ $h^{-1}$) | $\eta_{WL}$ (%) |
|---|---|---|---|
| Reference | 00 | 1.946 | - |
| PRQX | $10^{-6}$ | 0.403 | 79.3 |
| | $10^{-5}$ | 0.249 | 87.2 |
| | $10^{-4}$ | 0.165 | 91.5 |
| | $10^{-3}$ | 0.093 | 95.2 |

## PDP Investigation

Figure 2 displays PDP plots for C-S in the unfettered electrolyte using and without different PRQX amounts. Figure 2 reveals that when the PRQX is added to the reference electrolyte, the PDP plots shift to reduced current densities. Furthermore, the addition of PRQX to the acid solution significantly reduces the cathodic and anodic current densities, indicating that PRQX inhibits both the dissolution of the steel metal and the cathodic evolution of hydrogen [44].

As noticed, the lowered trend of the cathodic segment was greater than that of the anodic segment, suggesting that PRQX has a greater prevention impact from the cathodic reaction than the anodic reaction. Nevertheless, the cathodic portions are parallel, indicating that the PRQX has no effect on the mechanism of $H^+$ ions reduction and that hydrogen liberation happens predominantly through a charge transfer mechanism [45].

Table 2 provides the values of corrosion current density ($i_{corr}$), corrosion potential ($E_{corr}$), cathodic ($\beta_c$), and anodic ($\beta_a$) Tafel slopes that were acquired employing extrapolation of the linear sections of PDP graphs. It is widely agreed that the corrosion inhibitor is of the anodic or cathodic type when the $E_{corr}$ is more than 85 mV [46]. In our case, the maximum negative shift value of PRQX is 38 mV. As a result, PRQX is a mixed-type inhibitor for C-S in the acidic electrolyte. Additionally, the $i_{corr}$ value for the reference electrolyte was 1104.1 μA $cm^{-2}$, but it was only 25.3 μA $cm^{-2}$ in the presence of PRQX at $10^{-3}$ M. This difference may be ascribed to PRQX substances adsorbing on the C-S area, producing a barrier layer, and blocking the active sites. Furthermore, the $\beta_c$ values alter with PRQX introduction, pointing to a modification in the cathodic hydrogen evolution pathway, implying that PRQX significantly suppresses the corrosion process of C-S, and its performance increases with the amount. The restriction of the cathodic processes may be owing to the surface being covered with a monolayer as a result of the adsorbed PRQX chemicals [47]. However, contrasted with the electrolyte used as a comparison, the values of $\beta_a$ are significantly different in the existence of PRQX, suggesting that PRQX can influence the mechanism of the anodic sequence. The existence of N and O atoms in the quinoxaline-2-one rings which contain several lone pairs of electrons promotes the development of the Fe (II)-PRQX complex, altering the C-S dissolution process [48].

The $\eta_{PP}(\%)$ rises as the PRQX amount rises, peaking at 97.7% at $10^{-3}$ M, might be assigned to the molecule's high electron densities provoked by the abundance of π-electrons in the quinoxaline ring and lone pair electrons of N and O atoms.

## EIS Investigation

For C-S, the EIS investigations were conducted at 303 K in the unfettered electrolyte using and without PRQX to provide further information about the kinetic and C-S interface structure. Figure 3 and $S_1$ depict the Nyquist and Bode plots of PRQX. As per Fig. 3, the impedance spectra of

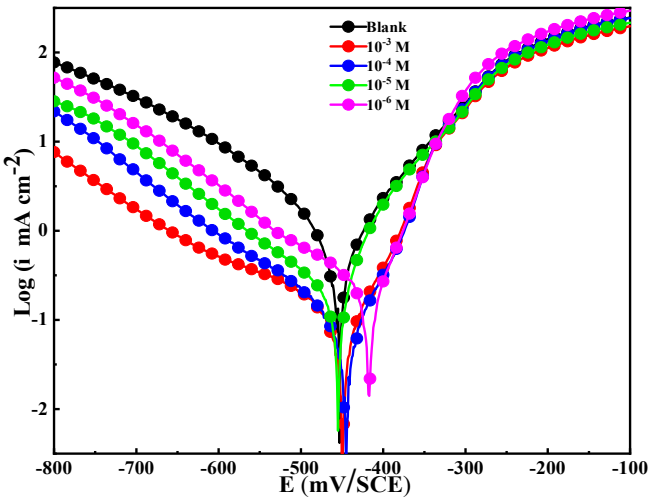


**Fig. 2.** PDP diagrams for C-S in the unfettered electrolyte using and without PRQX.

**Table 2.** PDP Indices and $\eta_{PP}(\%)$ for C-S Corrosion in Unfettered Electrolyte Using and without PRQX

| Electrolyte | C (M) | $-E_{corr}$ (mV $_{SCE}^{-1}$) | $-\beta_c$ (mV dec$^{-1}$) | $\beta_a$ (mV dec$^{-1}$) | $i_{corr}$ (μA cm$^{-2}$) | $\eta_{PP}(\%)$ |
|---|---|---|---|---|---|---|
| Reference | 00 | 456.3 | 155.4 | 112.8 | 1104.1 | - |
| PRQX | $10^{-6}$ | 418.4 | 139.2 | 56.1 | 171.8 | 84.4 |
| | $10^{-5}$ | 453.5 | 98.3 | 61.6 | 111.5 | 89.9 |
| | $10^{-4}$ | 444.2 | 109.1 | 79.7 | 58.8 | 94.6 |
| | $10^{-3}$ | 448.7 | 82.2 | 63.4 | 25.3 | 97.7 |

a reference electrolyte that contains and does not contain PRQX present a solitary capacitive loop, indicating that the corrosion of C-S occurs in a single charge transfer [49]. However, the forms of the EIS spectra in the restricted and unrestrained electrolytes remained similar, revealing that the existing mechanism was unchanged by the addition of PRQX. The large inhibition activity of PRQX is linked to the enlargement in the diameter of the EIS capacitive loop as the PRQX amount rises. Moreover, the Nyquist plots revealed somewhat depressed semicircular loops, which are attributable to dispersion effects, which are primarily due to the roughness and heterogeneity of the C-S area [50]. In the average frequency region of the bode plots (Fig. $S_1$), just a one-time constant is noticed. This behavior is attributed to a relaxing effect caused by PRQX adsorption on the steel area [51]. The adsorption of PRQX compounds on the C-S surface is also responsible for the rise in |Z| at low frequencies [52]. Furthermore, the appearance of a protective layer on the C-S interface may be ascribed to the noticeable rise in the phase angle value from 55.77° in the unrestrained electrolyte to 73.51° in the presence of $10^{-3}$ M of PRQX.

The equivalent circuit depicted in Fig. $S_2$ was utilized in order to correlate with the experiment's findings. It consisted of electrolyte resistance ($R_e$), polarization resistance ($R_p$), and the constant phase element (CPE). To better fit the experimental data, the CPE was utilized in the equivalent circuit instead of double-layer capacitance ($C_{dl}$). It is evident from Fig. 4 that there is a high degree of agreement between the simulation curves (red curves) and experimental data, indicating that the equivalent circuit depicted in Fig. $S_2$ is adequate for fitting the Nyquist graphs. The short fitness values Chi-square ($\chi^2 \approx 0.001$) in Table 3 reflect a strong consistency between the fitted and experiment data. The CPE impedance function is outlined as follows [53]:

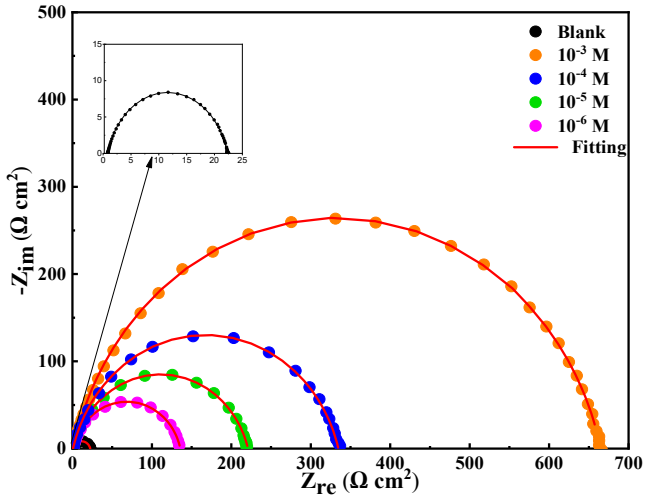


**Fig. 3.** EIS graphs for C-S in unfettered electrolyte using and without PRQX.

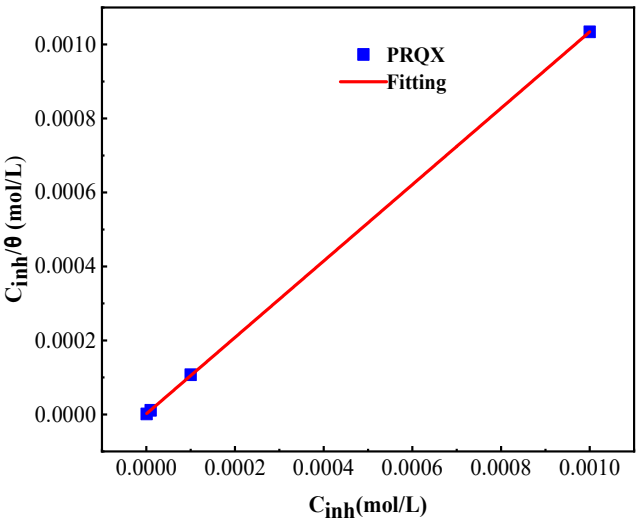


**Fig. 4.** Langmuir plot for the PRQX adsorption on the C-S in the acidic electrolyte at 303 K.

$$Z_{CPE} = \left( \frac{1}{\mathrm{Q}(i\omega)^{n}} \right) \quad (9)$$

Where Q, *i*, ω, and *n* respectively represent the CPE constant, imaginary number, angular frequency (ω = 2π*f*, where *f* is the frequency), and phase shift.

Additionally, the following equation links the CPE to the $C_{dl}$ [51]:

$$C_{dl} = \left( \mathrm{Q} R_p^{1-n} \right)^{1/n} = \mathrm{Q} \left( 2\pi f_{\max} \right)^{n-1} \quad (10)$$

Table 3 displays that the $R_p$ values are significantly greater than those of the reference electrolyte and rise with the amounts of PRQX, suggesting the creation of a protective layer at the C-S substrate [53]. As a consequence, the inhibition effectiveness increased as the inhibitor concentration increased, peaking at 96.7% at the highest amount, showing that PRQX was able to successfully inhibit the charge transfer behavior. When different concentrations of the PRQX inhibitor are added, the double layer capacity ($C_{dl}$) decreases from 116.2 μF cm$^{-2}$ for the reference (Blank) to 24.2 μF cm$^{-2}$ for the PRQX inhibitor ($10^{-3}$ M). Much research has been done on the interaction processes governing metal inhibition in an attempt to understand this characteristic [54,55]. These results show that as the inhibitor is adsorbed, the double layer capacity reduces and the organic film thickness increases according to the Helmholtz model formula:

$$\mathrm{C_{dl}} = \frac{\varepsilon\varepsilon_0}{\mathrm{d}}\mathrm{S} \quad (11)$$

Where d is the deposit's thickness, S is the electrode's usable area, $\varepsilon_0$ stands for the vacuum permittivity, and ε is the dielectric constant.

On the basis of this expression, the decrease in $C_{dl}$ may also come from a reduction in the dielectric constant ε, indicating that PRQX works by adsorption onto the C-S surface at the metal/solution interface [56]. Additionally, a reduction in the C-S surface's heterogeneity is responsible for an elevation in n values in the presence of PRQX. Notably, the $\eta_{EI}(\%)$ value derived using EIS exhibited the same pattern as the values derived from PDP and weight loss measures.

## Adsorption Isotherms

Organic molecules restrain metal dissolution after being adsorbed onto the metal/solution interface. As a result, it is essential to look into the adsorption properties of the PRQX compounds on the C-S interface. Adsorption isotherms are often regarded as one of the relevant criteria for determining inhibitor properties since they offer fundamental details on the interaction of the PRQX and the C-S [57]. In the current investigation, several adsorption isotherm models were examined, including the Langmuir, Freundlich, and Temkin isotherms, and the Langmuir adsorption isotherm was observed to offer the most precise clarification of the adsorption conduct of the studied PRQX. The equation of this model is the next [58]:

$$\frac{C_{\mathrm{inh}}}{\theta} = \frac{1}{K} + C_{\mathrm{inh}} \quad (12)$$

Where $C_{inh}$, $K$, and $(\theta = \eta_{EI}/100)$ are the PRQX dose, the equilibrium adsorption constant, and the surface coverage, respectively.

**Table 3.** EIS Indices for C-S in the Unfettered Electrolyte Using and without PRQX

| Electrolyte | $C$ (M) | $R_e$ (Ω cm$^2$) | $R_p$ (Ω cm$^2$) | $10^6 \times Q$ (Ω$^{-1}$ s$^n$ cm$^{-2}$) | $n$ | $C_{\mathrm{dl}}$ (μF cm$^{-2}$) | $\chi^2$ | $\eta_{EI}$ (%) | $\theta$ |
|---|---|---|---|---|---|---|---|---|---|
| Reference | 00 | 0.83 | 21.57 | 293.9 | 0.845 | 116.2 | 0.002 | - | - |
| PRQX | $10^{-6}$ | 0.84 | 140.2 | 86.7 | 0.848 | 39.3 | 0.001 | 84.6 | 0.846 |
| | $10^{-5}$ | 0.86 | 220.8 | 74.6 | 0.851 | 36.4 | 0.004 | 90.2 | 0.902 |
| | $10^{-4}$ | 0.91 | 333.9 | 56.5 | 0.858 | 29.3 | 0.004 | 93.3 | 0.933 |
| | $10^{-3}$ | 0.95 | 662.2 | 42.5 | 0.864 | 24.2 | 0.006 | 96.7 | 0.967 |

linear correlation coefficient ($R^2$) around one, implying that the adsorption of PRQX adheres to the Langmuir isotherm. The value of $K$ could be computed using the intercept of the last curve, which is used to estimate the free energy of adsorption $\Delta G^{\circ}_{ads}$ as [58]:

$$\Delta G^{\circ}_{ads} = -RT \times ln(55.5K) \quad (13)$$

where 55.5, *R,* and *T* are the water concentration, gas constant, and 303 K temperature, respectively.

The higher the K value, the stronger the adsorption of the inhibitor on the metal surface [59]. It is recognized that when $\Delta G^{\circ}_{ads}$ > -20 kJ mol$^{-1}$, inhibitor molecules can be located on the C-S substrate by electrostatic interactions (physisorption), whereas when $\Delta G^{\circ}_{ads}$ < -40 kJ mol$^{-1}$, inhibitor adsorption occurs through the creation between coordination bonds (chemisorption) of inhibitor molecules and the C-S substrate. In cases where -40 kJ mol$^{-1}$ < $\Delta G^{\circ}_{ads}$ < -20 kJ mol$^{-1}$, inhibitor adsorption occurs through both physisorption and chemisorptions [59]. In our case, the value of $\Delta G^{\circ}_{ads}$ is equal to -43.86 kJ mol$^{-1}$ which implies the adsorption of PRQX on the C–S substrate is principally through chemisorption.

## Influence of Temperature

The temperature's influence on C-S corrosion in the unfettered electrolyte using and without $10^{-3}$ M of PRQX was investigated using PDP assays at temperatures that varied from 303 to 333 K (Fig. $S_3$). Table 4 and Fig. $S_3$ display that when the temperature rises, the $i_{corr}$ rises in both unrestrained and inhibited electrolytes, and that the rise in the unfettered electrolyte is larger than the increase in the inhibited electrolytes, signifying that the increase in temperature is sluggish the adsorption molecules of PRQX on the C-S interface. The mediocre drop in performance with the presence of PRQX at a temperature range of 9.3% suggests PRQX's significant inhibitory capability and low-temperature dependency [60].

The Arrhenius and the transition state equations were employed to assess the corrosion rate of C-S in view of examining in-depth the temperature effect on the adsorption mechanism of PRQX. The equations are as follows [61]:

$$i_{corr} = A \times \exp\left(-E_a / RT\right) \quad (14)$$

$$ln\left(i_{corr}/T\right) = ln\left(R/Nh\right) + \left(\Delta S_a/R\right) - \left(\Delta H_a/RT\right) \quad (15)$$

where $A$ denotes the pre-exponential constant, $\Delta S_a$ denotes the apparent activation entropy, $h$ denotes Plank's constant, $\Delta H_a$ denotes the apparent activation enthalpy, $N$ denotes Avogadro's number, and $E_a$ denotes the apparent activation energy.

Table 5 displayed the $E_a$ values obtained from the slope of Arrhenius plots using and without PRQX (Fig. 5). The $E_a$ value with PRQX is bigger compared to the unfettered electrolyte; this finding may be connected to the

**Table 4.** PDP Indices of C-S Corrosion in Unfettered Electrolyte Using and without $10^{-3}$ M of PRQX at Different Temperatures

| Electrolyte | T (K) | $-E_{corr}$ (mV SCE$^{-1}$) | $-\beta_c$ (mV dec$^{-1}$) | $\beta_a$ (mV dec$^{-1}$) | $i_{corr}$ (μA cm$^{-2}$) | $\eta_{PP}$(%) |
|---|---|---|---|---|---|---|
| Reference | 303 | 456.3 | 155.4 | 112.8 | 1104.1 | - |
| | 313 | 423.5 | 131.3 | 91.3 | 1477.4 | - |
| | 323 | 436.3 | 117.8 | 91.4 | 2254.0 | - |
| | 333 | 433.3 | 134.6 | 103.9 | 3944.9 | - |
| PRQX | 303 | 448.7 | 82.2 | 63.4 | 25.3 | 97.7 |
| | 313 | 441.5 | 73.6 | 50.9 | 83.7 | 94.3 |
| | 323 | 441.8 | 80.2 | 44.7 | 170.5 | 92.4 |
| | 333 | 420.1 | 91.6 | 47.6 | 458.1 | 88.4 |

**Table 5.** The Activation Indices of C-S Corrosion in Unfettered Electrolyte Alone and PRQX

| Electrolyte | $E_a$ (kJ mol$^{-1}$) | $\Delta H_a$ (kJ mol$^{-1}$) | $\Delta S_a$ (J mol$^{-1}$ K$^{-1}$) |
|---|---|---|---|
| Reference | 35.4 | 32.8 | -79.2 |
| PRQX | 78.9 | 76.3 | 34.1 |

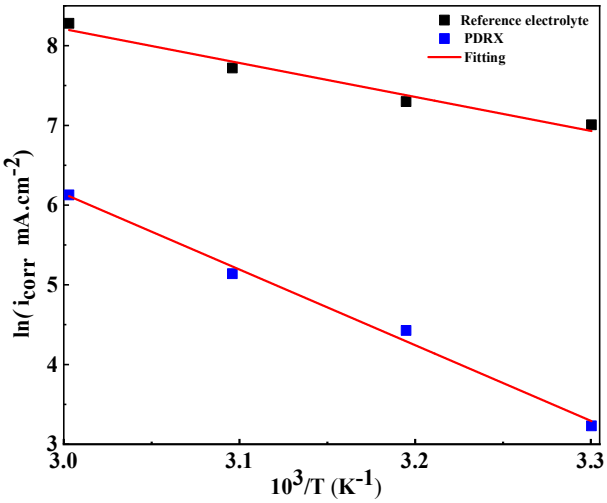


**Fig. 5.** Arrhenius graphs for C-S in the unfettered electrolyte alone with PRQX.

physisorption phenomena and a slowing of the corrosion rate, as stated in the literature [62]. Figure 6 depicts the alternative Arrhenius plots using and without PRQX. The $\Delta S_a$ and $\Delta H_a$ values were calculated using the intercept and the slope of the straight graphs, and the findings are displayed in Table 5. The positive sign for $\Delta H_a$ indicates the endothermic nature during the degradation of C-S [63]. As a result, a rise in temperature helps C-S dissolve. Furthermore, the addition of PRQX raised the value of $\Delta H_a$, proving that the adsorption of PRQX onto the C-S/electrolyte interface makes it more difficult for C-S to dissolve. In general, the $\Delta S_a$ it is used to characterize the system's disorder or order. However, the $\Delta S_a$ value is negative in the unfettered electrolyte and tends to be positive and greater in the existence of PRQX. This demonstrates a rise in disorder during the conversion of reactants into activated complexes [64]. Additionally,

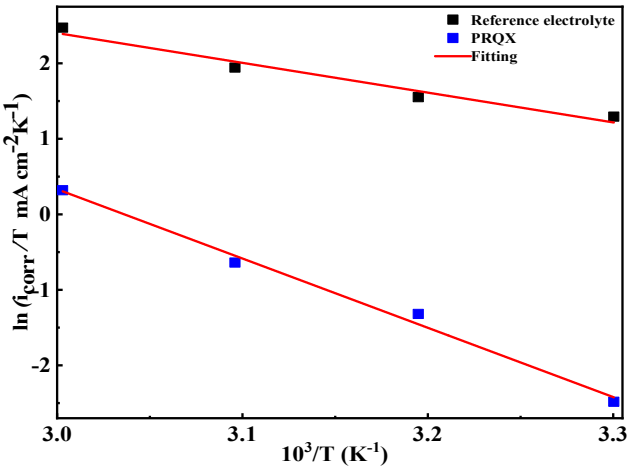


**Fig. 6.** Alternative Arrhenius graphs for C-S in unfettered electrolyte alone and PRQX.

this might be associated with PRQX molecule adsorption followed by water molecule desorption from the C-S surface.

## SEM micrographs and EDX spectra

The C-S surface was observed by SEM in the unfettered electrolyte containing and without 0.001 M PRQX after 24 h of plunging. The polished C-S surface has numerous scratches left behind from the polishing process (Fig. 7a). When the C-S substrate was submerged in the unrestricted electrolyte, large holes emerged over the whole surface (Fig. 7b). When PRQX was introduced to the acidic electrolyte (Fig. 7b), the dissolution of the C-S substrate was considerably reduced, signifying that the PRQX compounds were deposited on the C-S substrate and formed a protective layer.

The EDX spectra for C-S under various conditions are depicted in Fig. 7. From the polished C-S surface (Fig. 7a), it can be seen a large peak of iron and minor peaks corresponding to C-S chemical makeup. Strong characteristic peaks of Cl and O, components of HCl electrolyte and Fe oxide, are observed in the EDX spectrum of Fig. 7b after C-S submerging in the acidic electrolyte, suggesting the gathering of corrosion products on the C-S substrate. The corresponding peaks of corrosion products almost disappeared, and the Cl peak was greatly diminished in the presence of PRQX (Fig. 7c). In a nutshell, the SEM/EDX data reveal that PRQX has a significant inhibitory impact on C-S corrosion in acidic electrolyte.

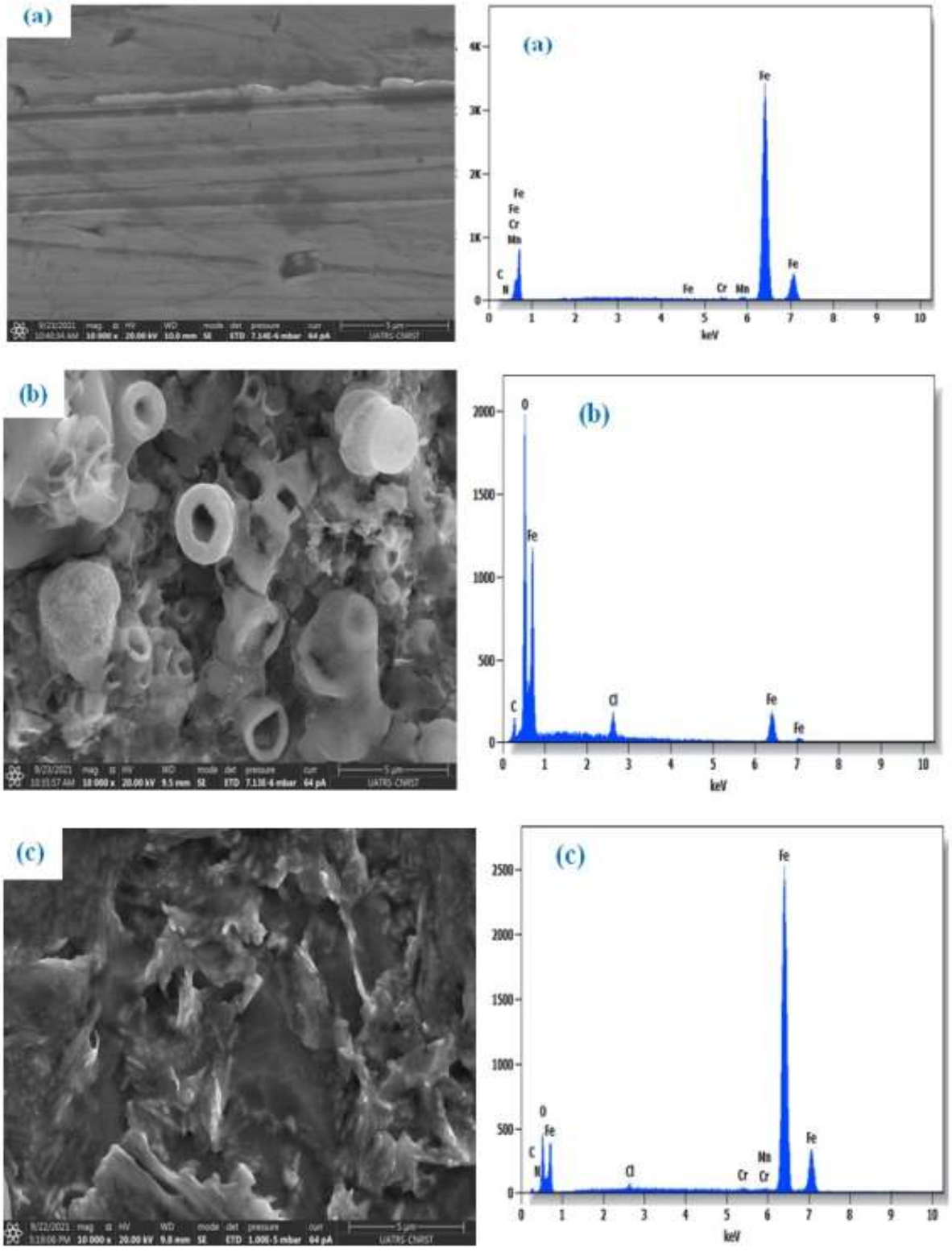


**Fig. 7.** SEM/EDX photographs acquired directly post-polishing (a), 24 h after submerging in the acidic electrolyte (b), and 24 h after submerging in the acidic electrolyte containing $10^{-3}$ M of PRQX (c).

## Electrolyte Analysis

To prove the potential for complex (PRQX-Fe(II)) development, UV-visible absorption spectra obtained from a 1 M HCl solution containing $10^{-3}$ M of PRQX were recorded before and after 72 h of C-S substrate submerging at 303 K and are provided in Fig. 8. According to earlier studies, a shift in the placement of an absorbance peak or a variation in absorption intensity suggest the development of a complex of two species in electrolyte [65]. The absorption spectrum of the electrolyte including $10^{-3}$ M of PRQX post-C-S submerging (blue curve) exhibits peaks at 207 nm and 260 nm, that are assigned to the π-π* transition of the aromatic systems (phenyl and quinoxaline) of the PRQX, and another peak at 308 nm, which corresponds to an n-π* transition involving the lone pair of electrons on the oxygen (Ketone) and nitrogen atoms. After 72 h of C-S submerging, it appears that except for the first peak, the others have undergone a redshift with a rise in absorbance (red curve). These variations reveal that interactions between PRQX and $Fe^{2+}$ in the acidic electrolyte have occurred.

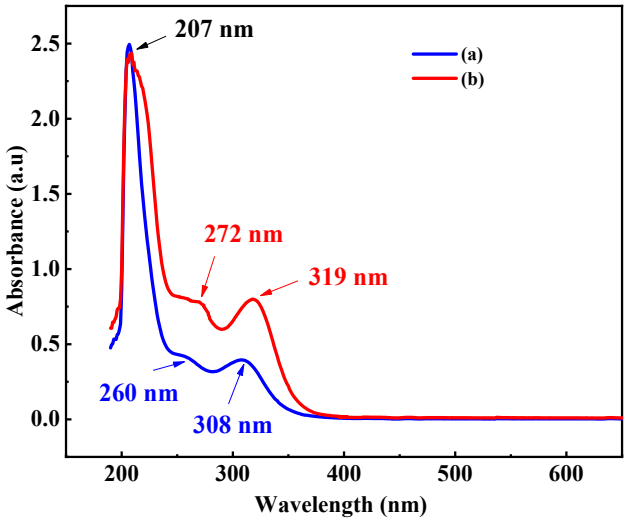


**Fig. 8.** UV-visible spectrum for PRQX in the acidic electrolyte before (blue curve (a)) and after (red curve (b)) 72 h of C-S substrate submerging.

## DFT Study

There are maps of electrostatic potential (MEP) and the electronic distributions of HOMO and LUMO in Fig. 9. The structure minimization (most stable/lowest energy) in the ground state (GS) is shown. The structure shown in this figure does not display negative frequencies in the Gaussian 09 file, reflecting this well-optimized representation. This leads to a better spreading out of the HOMO and LUMO electron densities at this structure level. As a result, FMO (HOMO/LUMO) distributions are found all over the optimized PRQX structure. The way this molecule behaves electronically suggests that it has a lot of places where it can react with other molecules both locally and globally (donor-attractor effect).

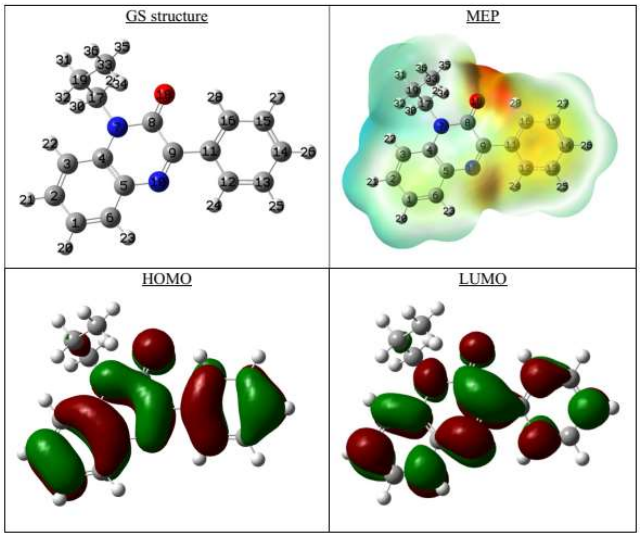


**Fig. 9.** Optimized state structure, MEP, HOMO, and LUMO of the PRQX.

Chemical quantum descriptors are numerical values that describe the electronic structure, bonding, and other molecular properties of chemical systems based on quantum calculations. These descriptors can be used to predict and understand chemical properties and reactions, and they are commonly used in computational chemistry, materials science, and drug discovery. The overall reactivity of these quantum descriptors is gathered in Table 6.

The energy gap (ΔE) is the parameter of most interest for the chemical reactivity of a PRQX molecule. The value of ΔE (3.851 eV) is identified as having the lowest energy gap, suggesting that it should have the highest reactivity and, therefore, the best inhibitory properties of the molecule studied [66,67]. $E_{HOMO}$ is closely associated with the

**Table 6.** Chemical Descriptors of the PRQX Molecule

| Descriptors of the PRQX | $E_{HOMO}$ (eV) | $E_{LUMO}$ (eV) | $\Delta E$ (eV) | $\chi$ (eV) | $\eta$ (eV) | $\Delta N_{110}$ |
|---|---|---|---|---|---|---|
| | -5.874 | -2.023 | 3.851 | 3.948 | 1.925 | 0.226 |

chemical responsiveness of the compound represented by the electron donor effect. The energy value of the LUMO determines the molecule's ability to accept electrons. A low LUMO value indicates a higher acceptor effect [68]. The highest $E_{HOMO}$ value (-5.874 eV) and the lowest $E_{LUMO}$ value (-2.023 eV) are the most favorable for chemical responsiveness. An expression used in quantum physics, electronegativity ($\chi$), describes the tendency of an atom to pull electrons towards itself in the structure of a molecule. In addition, a comparison of the two electronegativity energy values for the iron atom ($\chi_{Fe}$ (110) = 4.82 eV) and the inhibitor molecule studied (3.948 eV) shows a probable interaction.

In quantum chemistry, the term "overall hardness" ($\eta$) is used to describe a molecule's resistance to electronic changes like electron donation or acceptance. Hardness is a measure of the energy required to make an electronic change in a molecule. A molecule with high hardness requires more energy to accept or donate an electron compared to a molecule with low hardness. Hardness is related to the reactivity of a molecule towards electron transfer, where a high hardness indicates low reactivity and vice versa [68]. In the case studied, the minimum $\eta$ value (1.925 eV) of the PRQX molecule justifies well the maximum value of the inhibitory efficacy of this molecule obtained experimentally 98% at $10^{-3}$ M. The number of electrons released from the optimized PRQX to the vacant orbitals “d” of the iron d is quantified using $\Delta N_{110}$, a high value of this descriptor denotes a large electron donor effect [68]. The value of 0.226 ($\Delta N_{110}$) informs that PRQX can easily donate electrons to form coordination obligations with the C-S substrate.

The total selectivity method based on the use of Fukui indices (Functions) can be used to define the atoms involved in nucleophilic (f(+)) and electrophilic (f(-)) attacks. The calculation used to determine the most relevant sites was carried out in a work published by Benhiba and al. [69]. The data of this method are regrouped in Table 7. Atoms with a high density of Fukui functions are, C(1), C(2), C(4), C(5), N(7), and O(18) for *f(-)*; C(2), C(6), C(9), N(10), and O(18) for *f(+)*, responsible for the local reactivity and provide a greater number of coordination bonds, which favors adsorption of PRQX to the C-S support.

**Table 7.** Fukui Indices (*f(+)* and *f(-)*) of the Atoms for PRQX Molecule

| Atoms | *f(-)* | *f(+)* |
|---|---|---|
| C (1) | 0.068 | 0.036 |
| C (2) | 0.054 | 0.059 |
| C (3) | 0.037 | 0.036 |
| C (4) | 0.050 | 0.031 |
| C (5) | 0.056 | 0.028 |
| C (6) | 0.034 | 0.050 |
| N (7) | 0.046 | 0.035 |
| C (8) | 0.040 | 0.042 |
| C (9) | 0.043 | 0.095 |
| N (10) | 0.039 | 0.104 |
| C (11) | 0.028 | 0.021 |
| C (12) | 0.032 | 0.036 |
| C (13) | 0.023 | 0.025 |
| C (14) | 0.045 | 0.046 |
| C (15) | 0.027 | 0.026 |
| C (16) | 0.028 | 0.034 |
| C (17) | 0.011 | 0.010 |
| O (18) | 0.100 | 0.055 |
| C (19) | 0.007 | 0.005 |
| C (33) | 0.003 | 0.002 |

## MDS Study

The use of computational approaches, such as molecular dynamics simulations, can be helpful in predicting and understanding the adsorption configuration of molecules on surfaces. In addition, MDS is a powerful tool for investigating the behavior of molecular systems [70].

The goal of this investigation is to examine and comprehend how the PRQX molecule in its neutral form interacts with the atomic surface of iron (Fe(110)). Furthermore, Fig. 10 reproduces the best adsorption configuration PRQX onto the Fe(110) substrate. As stated in these two views, $H_3O^+$ and $Cl^-$ approach the Fe(110) surface, an indication of possible corrosion by acid solution. In addition, the optimized pattern of the molecule takes up a substantial part of the Fe(110) and no $H_3O^+$ and $Cl^-$ approaches where PRQX has been adsorbed. Apparently, the fact that this adsorption property informs that there are several active acceptor/donor sites that contribute to the rise of the inhibition effectiveness of the mentioned substance.

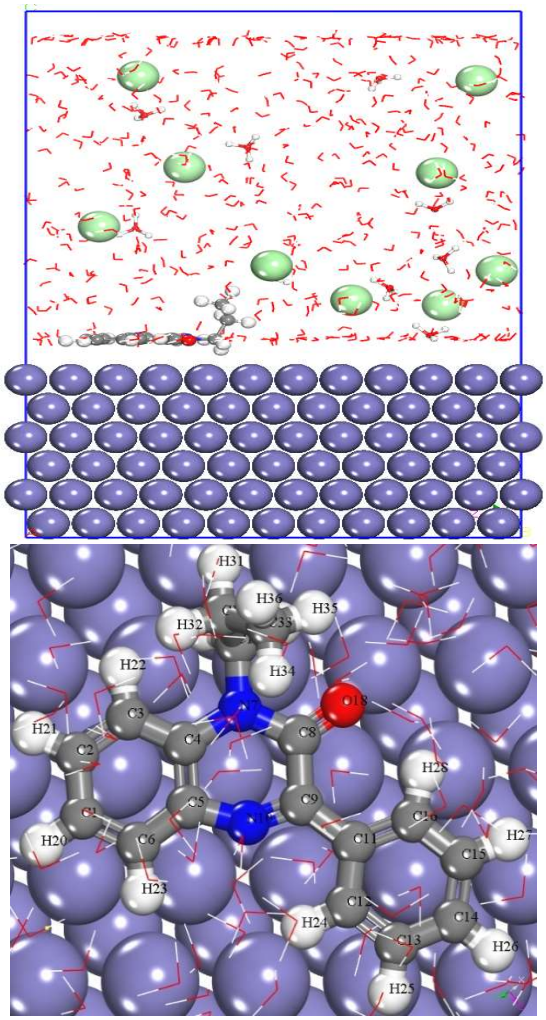


**Fig. 10.** Side (left) and top (right) views of the PRQX /Fe(110) system.

The $E_{interaction}$ and $E_{binding}$ values are defined by the two equations hereunder [71]:

$$E_{interaction} = E_{total} - (E_{surface + solution} + E_{inhibitor}) \text{ and } E_{binding} = - E_{interaction} \quad (16)$$

The low value of $E_{interaction}$ approves the interaction of PRQX with the interacting iron atoms, while the higher values of $E_{binding}$ testify to large adsorption [71].

The values of these two descriptors for the system are calculated, depending on the comparative study on the comparable study that the most negative value of PRQX /Fe(110) (-893.587 kJ $mol^{-1}$) reflects a larger interaction, while the highest value of $E_{binding}$ (893.587 kJ $mol^{-1}$) of this system indicates that the target molecule strongly binds to the investigated atomic layer.

The radial distribution function (RDF) approach is used to clarify the type of bonds that exist between the investigated inhibitor and the Fe atoms. The latter is a valuable tool for the determination of the Fe-PRQX interatomic distance [72]. The published literature confirmed that the likelihood of chemical adsorption was higher when the bond length was less than 3.5 Å. By contrast, physical adsorption is more probable [73]. In Fig. $S_4$, the spectral data from this method are illustrated. The first peaks reveal that the bond lengths (PRQX-Fe) are less than 3.5 Å.

## CONCLUSION

Employing systematic techniques and characterization instruments, a study was carried out into the ability of quinoxalinone (PRQX) to prevent C-S corrosion in an acid electrolyte, as well as its corrosion inhibition mechanism. The outcomes facilitate the establishment of the next conclusions:

- PRQX exhibits strong C-S corrosion inhibition in the acidic electrolyte, and their effectiveness grows with concentration, reaching 97.7% at $10^{-3}$ M.
- According to the PDP profiles, the PRQX significantly blocks both cathodic hydrogen generation and anodic metal dissolution processes, establishing that it is a mixed-type inhibitor with a propensity for the cathode. The PRQX's presence increases Rp values while decreasing the constant phase element of the double layer ($C_{dlCPE}$), as determined by

EIS assessments, suggesting the inhibitor's inhibitory influence on C-S corrosion.

- The Langmuir adsorption isotherm is appropriate with the chemisorption process of PRQX adsorption on the C-S interface.
- Surface and electrolyte analyses (SEM, EDX, and UV-visible) suggested the PRQX adsorption on the C-S interface.
- Conceptual methods show that PRQX adheres well to the chosen surface.

## REFERENCES


[1] Zheng, H.; Zhang, B.; Wang, X.; Lu, Y.; Li, F.; Li, C., Improved corrosion resistance of carbon steel in soft water with dendritic-polymer corrosion inhibitors. *Chem. Eng. J.* **2023**, *452* 139043, DOI: 10.1016/j.cej.2022.139043

[2] Zarrouk, A.; Zarrok, H.; Ramli, Y.; Bouachrine, M.; Hammouti, B.; Sahibed-dine, A.; Bentiss, F. , Inhibitive properties , adsorption and theoretical study of corrosion inhibitor for carbon steel in hydrochloric acid solution. *J. Mol. Liq.* **2016**, *222*, 239-252, DOI: 10.1016/j.molliq.2016.07.046.

[3] El Faydy, M.; Benhiba, F.; Lakhrissi, B.; Touhami, M. E.; Warad, I.; Bentiss, F.; Zarrouk, A., The inhibitive impact of both kinds of 5-isothiocyanatomethyl-8-hydroxyquinoline derivatives on the corrosion of carbon steel in acidic electrolyte. *J. Mol. Liq.* **2019**, *295*, 111629. DOI: 10.1016/j.molliq.2019.111629.

[4] Allali, M.; Ichou, Y.; Allali, N.; Zarrouk, A.; Habbadi, N., Synthesis and full characterization of new symmetric bis-triazol ligand and complexes with divalent Nickel, Copper and Zinc. *J. Mater. Environ. Sci.* **2016**, *7*, 2042-2050.

[5] Lazrak, J.; Ech-chihbi, E.; El Ibrahimi, B.; El Hajjaji, F.; Rais, Z.; Tachihante, M.; Taleb, M., Physicochemical and Engineering Aspects Detailed DFT/MD simulation , surface analysis and electrochemical computer explorations of aldehyde derivatives for mild steel in 1.0 M HCl. *Colloids Surfaces A Physicochem. Eng. Asp.* **2022**, *632*, 127822, DOI: 10.1016/j.colsurfa.2021.127822.

[6] El Faydy, M.; Benhiba, F.; Warad, I.; About, H.; Saoiabi, S.; Guenbour, A.; Bentiss, F.; Lakhrissi, B.; Zarrouk, A., Experimental and theoretical investigations of two quinolin-8-ol derivatives as inhibitors for carbon steel in 1 M HCl solution. *J. Phys. Chem. Solids.* **2022**, *165*, 110699, DOI: 10.1016/j.jpcs.2022.110699.

[7] Sengupta, S.; Murmu, M.; Murmu, N. C.; Banerjee, P., Adsorption of redox-active Schiff bases and corrosion inhibiting property for mild steel in 1 M $H_2SO_4$: Experimental analysis supported by *ab initio* DFT, DFTB and molecular dynamics simulation approach. *J. Mol. Liq.* **2021**, *326*, 115215, DOI: 10.1016/j.molliq.2020.115215.

[8] Tripathy, D. B.; Murmu, M.; Banerjee, P.; Quraishi, M. A., Palmitic acid based environmentally benign corrosion inhibiting formulation useful during acid cleansing process in MSF desalination plants. *Desalination*. **2019**, *472*, 114128, DOI: 10.1016/j.desal.2019.114128.

[9] El Faydy, M.; Benhiba, F.; Timoudan, N.; Lakhrissi, B.; Warad, I.; Saoiabi, S.; Guenbour, A.; Bentiss, F.; Zarrouk, A., Experimental and theoretical examinations of two quinolin-8-ol-piperazine derivatives as organic corrosion inhibitors for C35E steel in hydrochloric acid, *J. Mol. Liq.* **2022**, *354*, 118900, DOI: 10.1016/j.molliq.2022.118900.

[10] Zarrok, H.; Zarrouk, A.; Salghi, R.; Oudda, H.; Hammouti, B.; Ebn Touhami, M.; Bouachrine, M.; Pucci, O. H., A combined experimental and theoretical study on the corrosion inhibition and adsorption behaviour of quinoxaline derivative during carbon steel corrosion in hydrochloric acid. *Port. Electrochim. Acta.* **2012**, *30*, 405-417, DOI: 10.4152/pea.201206405.

[11] Singh, D.; Singh, P.; Quraishi, M.A., Quinoxaline derivatives as efficient corrosion inhibitors : Current status , challenges and future perspectives, *J. Mol. Liq.* **2020**, *320*, 114387, DOI: 10.1016/j.molliq.2020.114387.

[12] Zarrok, H.; Zarrouk, A.; Salghi, R.; Ebn Touhami, M.; Oudda, H.; Hammouti, B.; Touir, R.; Bentiss, F.; Al-Deyab, S. S., Corrosion Inhibition of C38 Steel in Acidic Medium Using N-1 Naphthylethylenediamine Dihydrochloride Monomethanolate. *Int. J. Electrochem. Sci.* **2013**, *8*, 6014-6032. https://doi.org/10.1016/S1452-3981(23)14736-5.

[13] Zarrouk, A.; Zarrok, H.; Salghi, R.; Bouroumane, N.; Hammouti, B.; Al-Deyab, S. S.; Touzani, R., The Adsorption and Corrosion Inhibition of 2-[Bis-(3,5-

dimethyl-pyrazol-1-ylmethyl)-amino]-pentanedioic Acid on Carbon Steel Corrosion in 1.0 m HCl. *Int. J. Electrochem. Sci.* **2012**, *7*, 10215-10232. https://doi.org/10.1016/S1452-3981(23)16271-7.

[14] Zarrouk, A.; Messali, M.; Zarrok, H.; Salghi, R.; Al-Sheikh Ali, A.; Hammouti, B.; Al-Deyab, S. S.; Bentiss, F., Synthesis, Characterization and Comparative Study of New Functionalized Imidazolium-Based Ionic Liquids Derivatives Towards Corrosion of C38 Steel in Molar Hydrochloric Acid. *Int. J. Electrochem. Sci.* **2012**, *7*, 6998-7015. https://doi.org/10.1016/S1452-3981(23)15764-6.

[15] Zarrouk, A.; Hammouti, B.; Zarrok, H.; Salghi, R.; Dafali, A.; Bazzi, Lh.; Bammou, L.; Al-Deyab, S. S., Electrochemical impedance spectroscopy and weight loss study for new pyridazine derivative as inhibitor for copper in nitric acid. *Der Pharma Chem.* **2012**, *4* (1), 337-346.

[16] Zarrok, H.; Salghi, R.; Zarrouk, A.; Hammouti, B.; Oudda, H.; Bazzi, Lh.; Bammou, L.; Al-Deyab, S. S., Investigation of the Inhibition Effect of N-1-Naphthylethylenediamine Dihydrochloride Monomethanolate on the C38 Steel Corrosion in 0.5M $H_2SO_4$. *Der Pharma Chem.* **2012**, *4* (1), 407-416.

[17] Zarrouk, A.; Hammouti, B.; Dafali, A.; Zarrok, H., L-Cysteine methyl ester hydrochloride: A new corrosion inhibitor for copper in nitric acid. *Der Pharma Chem.* **2011**, *3* (4), 266-274.

[18] Zarrouk, A.; Chelfi, T.; Dafali, A.; Hammouti, B.; Al-Deyab, S. S.; Warad, I.; Benchat, N.; Zertoubi, M., Comparative Study of new Pyridazine Derivatives Towards Corrosion of Copper in Nitric Acid: Part-1. *Int. J. Electrochem. Sci.* **2010**, *5*, 696-705. https://doi.org/10.1016/S1452-3981(23)15316-8.

[19] Saraswat, V.; Kumari, R.; Yadav, M., Novel carbon dots as efficient green corrosion inhibitor for mild steel in HCl solution: Electrochemical, gravimetric and XPS studies. *J. Phys. Chem. Solids.* **2022**, *160*, 110341, DOI: 10.1016/j.jpcs.2021.110341.

[20] El Faydy, M.; Lakhrissi, B.; Jama, C.; Zarrouk, A.; Olasunkanmi, L. O.; Ebenso, E. E.; Bentiss, F., Electrochemical, surface and computational studies on the inhibition performance of some newly synthesized 8-hydroxyquinoline derivatives containing benzimidazole moiety against the corrosion of carbon steel in phosphoric acid environment. *J. Mater. Res. Technol.* **2019**, *9* (1), 727-748, DOI: 10.1016/j.jmrt.2019.11.014

[21] Benhiba, F.; Hsissou, R.; Benzekri, Z.; Belghiti, M. E.; Lamhamdi, A.; Bellaouchou, A.; Guenbour, A., Nitro substituent effect on the electronic behavior and inhibitory performance of two quinoxaline derivatives in relation to the corrosion of mild steel in 1 M HCl. *J. Mol. Liq.* **2020**, *312*, 113367, DOI: 10.1016/ j.molliq.2020.113367.

[22] Sallam, E. R.; Aboulnaga, S. F.; Samy, A. M.; Beltagy, D. M.; El Desouky, J. M.; Abdel-Hamid, H.; Fetouh, H. A., Synthesis, characterization of new heterocyclic compound: pyrazolyl hydrazino quinoxaline derivative: 3-[5-(hydroxy1methyl)-1-phenylpyrazol-3-yl]-2-[2,4,5-trimethoxybenzylidine] hydrazonyl-quinoxaline of potent antimicrobial, antioxidant, antiviral, and antitumor activity. *J. Mol. Struct.* **2023**, *1271*, 133983, DOI: 10.1016/j.molstruc.2022.133983.

[23] Meka, G., Chintakunta, R., Analgesic and anti-inflammatory activity of quinoxaline derivatives: Design synthesis and characterization. *Results Chem.* **2023**, *5*, 100783, DOI: 10.1016/j.rechem.2023.100783.

[24] Chahir, L.; El Faydy, M.; Abad, N.; Benhiba, F.; Warad, I.; Benmessaoud Left, D.; Zertoubi, M.; Allali, M.; Kaichouh, G.; Dikici, B.; Bellaouchou, A.; Ramli, Y.; Zarrouk, A., Corrosion Inhibition Effect of Quinoxaline Derivative on Carbon Steel in Hydrochloric Acid: Experimental and Theoretical Investigations, *J. Bio-Tribo-Corrosion.* **2024**, *10*, DOI: 10.1007/s40735-024-00840-6.

[25] Chauhan, D. S.; Singh, P.; Quraishi, M. A., Quinoxaline derivatives as efficient corrosion inhibitors: Current status, challenges and future perspectives. *J. Mol. Liq.* **2020**, *320*, 11438, DOI: 10.1016/ j.molliq.2020.114387.

[26] Saraswat, V.; Yadav, M., Computational and electrochemical analysis on quinoxalines as corrosion inhibitors for mild steel in acidic medium. *J. Mol. Liq.* **2020**, *297*,111883, DOI: 10.1016/j.molliq.2019.111883.

[27] Olasunkanmi, L. O.; Ebenso, E. E., Experimental and computational studies on propanone derivatives of quinoxalin-6-yl-4,5-dihydropyrazole as inhibitors of mild steel corrosion in hydrochloric acid. *J. Colloid Interface Sci.* **2020**, *561*, 104-116, DOI: 10.1016/

j.jcis.2019.11.097.

[28] Laabaissi, T.; Benhiba, F.; Missioui, M.; Rouifi, Z.; Rbaa, M.; Oudda, H.; Ramli, Y.; Guenbour, A.; Warad, I.; Zarrouk, A., Coupling of chemical, electrochemical and theoretical approach to study the corrosion inhibition of mild steel by new quinoxaline compounds in 1 M HCl. *Heliyon*. **2020**, *6* (5), e03939, DOI: 10.1016/ j.heliyon.2020.e03939.

[29] Benhiba, F.; Hsissou, R.; Benzekri, Z.; Echihi, S.; El-blilak, J.; Boukhris, S.; Bellaouchou, A., DFT/ electronic scale, MD simulation and evaluation of 6-methyl-2-(p-tolyl)-1,4-dihydroquinoxaline as a potential corrosion inhibition. *J. Mol. Liq.* **2021**, *335*, 116539, DOI: 10.1016/j.molliq.2021.116539.

[30] ASTM, Standard Practice for Preparing, Cleaning, and Evaluating Corrosion Test Specimens. Designation: G1-03, ASTM Spec. *Tech. Publ.* **2017**, 505-510, DOI: 10.1520/JTE20180585

[31] About, H.; El Faydy, M.; Benhiba, F.; Kerroum, Y.; Kaichouh, G.; Oudda, H.; Guenbour, A.; Lakhrissi, B.; Waradd, I.; Zarrouk, A., Experimental and empirical assessment of two new 8-hydroxyquinoline analogs as effective corrosion inhibitor for C22E steel in 1 M HCl. *J. Mol. Liq.* **2021**, *325*, 114644, DOI: 10.1016/ j.molliq.2020.114644.

[32] Bouassiria, M.; Laabaissi, T.; Benhiba, F.; El Faydy, M.; Fakhry, H.; Oudda, H.; Assouag, M.; Touir, R.; Guenbour, A.; Lakhrissi, B.; Warad, I.; Zarrouk, A., Corrosion inhibition effect of 5-(4-methylpiperazine)-methylquinoline-8-ol on carbon steel in molar acid medium. *Inorg. Chem. Commun.* **2021**, *123*, 108366, DOI: 10.1016/j.inoche.2020.108366.

[33] Fatah, A.; Timoudan, N.; Rbaa, M.; Benhiba, F.; Hsissou, R.; Safi, Z. S.; Warad, I.; AlObaid, A. A.; Al-Maswari, B. M.; Boutakiout, A.; Zarrok, H.; Lakhrissi, B.; Bellaouchou, A.; Jama, C.; Bentiss, F.; Oudda, H.; Zarrouk, A., Assessment of New Imidazol Derivatives and Investigation of Their Corrosion-Reducing Characteristics for Carbon Steel in HCl Acid Solution. *Coatings* **2023**, *13*, 1405. https://doi.org/10.3390/ coatings13081405

[34] Benhiba, F.; Benzekri, Z.; Guenbour, A.; Tabyaoui, M.; Bellaouchou, A.; Boukhris, S.; Oudda, H.; Warad, I.; Zarrouk, A., Combined electronic/atomic level computational, surface (SEM/EDS), chemical and electrochemical studies of the mild steel surface by quinoxalines derivatives anti-corrosion properties in 1 M HCl solution. *Chinese J. Chem. Eng.* **2020**, *28*, 1436-1458, DOI: 10.1016/j.cjche.2020.03.002.

[35] Laadam, G.; Benhiba, F.; El Faydy, M.; Titi, A.; Al-Gorair, A.S.; Alshareef, M.; Hawsawi, H.; Touzani, R.: Warad, I.; Bellaouchou, A.; Guenbour, A.; Abdallah, M.; Zarrouk, A., Anti-corrosion performance of novel pyrazole derivative for carbon steel corrosion in 1 M HCl: Computational and experimental studies. *Inorg. Chem. Commun.* **2022**, *145*, 109963, DOI: 10.1016/ j.inoche.2022.109963.

[36] Barrahi; A.; El Faydy, M.; Adlani L.; Benhiba, F.; Bazanov, D. R.; Lozinskaya, N. A.; Maatallah, M.; Warad, I.; Dikici, B.; Bellaouchou, A.; Zarrouk, A., Anticorrosive characteristics of imidazole derivative on carbon steel in 1 M HCl, **2024**, *14*, 193-212, DOI: 10.5599/jese.2136.

[37] Thoume, A.; Left, D. B.; Elmakssoudi, A.; Benhiba, F.; Zarrouk, A.; Benzbiria, N.; Warad, I.; Dakir, M.; Azzi, M.; Zertoubi, M., Chalcone oxime derivatives as new inhibitors corrosion of carbon steel in 1 M HCl solution. *J. Mol. Liq.* **2021**, *337*, 116398, DOI: 10.1016/ j.molliq.2021.116398.

[38] Quadri, T. W.; Olasunkanmi, L. O.; Fayemi, O. E.; Lgaz, H.; Dagdag, O.; Sherif, E. S. M.; Alrashdi, A. A.; Akpan, E. D.; Lee, H. S.; Ebenso, E. E., Computational insights into quinoxaline-based corrosion inhibitors of steel in HCl: Quantum chemical analysis and QSPR-ANN studies. *Arab. J. Chem.* **2022**, *15*, 103870, DOI: 10.1016/j.arabjc.2022.103870.

[39] El Faydy, M.; Benhiba, F.; Berisha, A.; Kerroum, Y.; Jama, C.; Lakhrissi, B.; Guenbour, A.; Warad, I.; Zarrouk, A., An experimental-coupled empirical investigation on the corrosion inhibitory action of 7-alkyl-8-Hydroxyquinolines on C35E steel in HCl electrolyte. *J. Mol. Liq.* **2020**, *317*, 113973, DOI: 10.1016/j.molliq.2020.113973.

[40] Hsissou, R.; Dagdag, O.; Abbout, S.; Benhiba, F.; Berradi, M.; El Bouchti, M.; Berisha, A.; Hajjaji, N.; Elharfi, A., Novel derivative epoxy resin TGETET as a corrosion inhibition of E24 carbon steel in 1.0 M HCl solution. Experimental and computational (DFT and MD

simulations) methods. *J. Mol. Liq.* **2019,** *284*, 182-192, DOI: 10.1016/j.molliq.2019.03.180.

[41] Materials Studio, Revision 8.0, Accelrys Inc., San Diego, USA , **2016**, DOI: 1259524417

[42] Andersen, H. C., Molecular dynamics simulations at constant pressure and/or temperature. *J. Chem. Phys*. **1980**, *72*, 2384-2393, DOI: 10.1063/1.1420460

[43] Nadi, I.; Belattmania, Z.; Sabour, B.; Reani, A.; Sahibed-dine, A.; Jama, C.; Bentiss, F., Sargassum muticum extract based on alginate biopolymer as a new efficient biological corrosion inhibitor for carbon steel in hydrochloric acid pickling environment: Gravimetric, electrochemical and surface studies. *Int. J. Biol. Macromol.* **2019**, *141*, 137-149, DOI: 10.1016/ j.ijbiomac.2019.08.253.

[44] Zhang, W.; Nie, B.; Li, H. J.; Li, Q.; Li, C.; Wu, Y. C., Inhibition of mild steel corrosion in 1 M HCl by chondroitin sulfate and its synergistic effect with sodium alginate. *Carbohydr. Polym.* **2021**, *260*, 117842, DOI: 10.1016/j.carbpol.2021.117842.

[45] Qiang, Y.; Guo, L.; Li, H.; Lan, X., Fabrication of environmentally friendly Losartan potassium film for corrosion inhibition of mild steel in HCl medium. *Chem. Eng. J.* **2021**, *406*, 126863, DOI: 10.1016/ j.cej.2020.126863.

[46] Nwankwo, H. U.; Akpan, E. D.; Olasunkanmi, L. O.; Verma, C.; Al-Mohaimeed, A. M.; Farraj, D. A. A.; Ebenso, E. E., N-substituted carbazoles as corrosion inhibitors in microbiologically influenced and acidic corrosion of mild steel: Gravimetric, electrochemical, surface and computational studies. *J. Mol. Struct.* **2021**, *1223*, 129328, DOI: 10.1016/j.molstruc.2020.129328.

[47] El Faydy, M.; Galai, M.; El Assyry, A.; Tazouti, A.; Touir, R.; Lakhrissi, B.; Ebn Touhami, M.; Zarrouk, A., Experimental investigation on the corrosion inhibition of carbon steel by 5-(chloromethyl)-8-quinolinol hydrochloride in hydrochloric acid solution. *Journal of Molecular Liquids.* **2016**, *219*, 396-404, DOI: 10.1016/ j.molliq.2016.03.056.

[48] Zhang, F.; Tang, Y.; Cao, Z; Jing, W.; Wu, Z.; Chen, Y., Performance and theoretical study on corrosion inhibition of 2-(4-pyridyl)-benzimidazole for mild steel in hydrochloric acid. *Corros. Sci.* **2012**, *61*, 1-9, DOI: 10.1016/j.corsci.2012.03.045.

[49] Kellal, R.; Benmessaoud Left, D.; Safi, Z. S.; Wazzan, N.; Al-Qurashi, O. S.; Zertoubi, M., A new approach for the evaluation of liquid waste generated from plant extraction process for the corrosion mitigation of carbon steel in acidic medium: Case of Chrysanthemum Coronarium stems, *J. Ind. Eng. Chem.* 2**023**, *125*, 370-389, DOI: 10.1016/j.jiec.2023.05.046.

[50] Jiang, Z.; Li, Y.; Zhang, Q.; Hou, B.; Xiong, W.; Liu, H.; Zhang, G., Purine derivatives as high efficient eco-friendly inhibitors for the corrosion of mild steel in acidic medium: Experimental and theoretical calculations. *J. Mol. Liq.* **2021**, *323*, 114809, DOI: 10.1016/ j.molliq.2020.114809.

[51] Al Garadi, W.; Jrajri, K.; El Faydy, M.; Benhiba, F.; El Ghayati, L.; Sebbar, N. K.; Essassi, E. M.; Warad, I.; Guenbour, A.; Bellaouchou, A.; Jama, C.; Alsalme, A.; Zarrouk, A., 4-Phenyl-decahydro-1H-1,5-benzodiazepin-2-one as novel and effective corrosion inhibitor for carbon steel in 1 M HCl solution: A combined experimental and empirical studies. *J. Indian Chem. Soc.* **2022**, *99*, 100742, DOI: 10.1016/j.jics.2022.100742.

[52] El Faydy, M.; Benhiba, F.; Warad, I.; About, H.; Saoiabi, S.; Guenbour, A.; Bentiss, F.; Lakhrissi, B.; Zarrouk, A., Experimental and theoretical investigations of two quinolin-8-ol derivatives as inhibitors for carbon steel in 1 M HCl solution. *J. Phys. Chem. Solids.* **2022**, *165*, 110699, DOI: 10.1016/j.jpcs.2022.110699.

[53] Anusuya, N.; Saranya, J.; Sounthari, P.; Zarrouk, A.; Chitra, S., Corrosion inhibition and adsorption behaviour of some bis-pyrimidine derivatives on mild steel in acidic medium. *J. Mol. Liq.* **2017**, *225*, 406-417, DOI: 10.1016/ j.molliq.2016.11.015.

[54] Benhiba, F.; Benzekri, Z.; Kerroum, Y.; Timoudan, N.; Hsissou, R.; Guenbour, A.; Belfaquir, M.; Boukhris, S.; Bellaouchou, A.; Oudda, H.; Zarrouk, A., Assessment of inhibitory behavior of ethyl 5-cyano-4-(furan-2-yl)-2-methyl-6-oxo-1,4,5,6-tetrahydropyridine-3-carboxylate as a corrosion inhibitor for carbon steel in molar HCl: Theoretical approaches and experimental investigation, *J. Indian Chem. Soc.* **2023**, 100, DOI: 10.1016/ J.JICS.2023.100916.

[55] Oubaaqa, M.; Ouakki, M.; Rbaa, M.; Elgendy, A.; Idouhli, R.; Maatallah, M.; Jarid, A.; Touhami, M. E.; Lakhrissi, B.; Zarrouk, A., Two pyran derivatives as

corrosion inhibitors for mild steel in HCl solution: Experimental and theoretical investigations, *Mater. Today Commun.* **2023**, *35*, 106188. DOI: 10.1016/J.MTCOMM.2023.106188.

[56] Alamshany, Z. M.; Ganash, A. A., Synthesis, characterization, and anti-corrosion properties of an 8-hydroxyquinoline derivative. *Heliyon*. **2019**, *5*, e02895, DOI: 10.1016/J.HELIYON.2019.E02895.

[57] Laadam, G.; El Faydy, M.; Benhiba, F.; Titi, A.; Amegroud, H.; Al-Gorair, A. S.; Hawsawi, H.; Touzani, R.; Warad, I.; Bellaouchou, A.; Guenbour, A.; Abdallah, M.; Zarrouk, A., Outstanding anti-corrosion performance of two pyrazole derivatives on carbon steel in acidic medium: Experimental and quantum-chemical examinations. *J. Mol. Liq.* **2023**, 121268, DOI: 10.1016/j.molliq.2023.121268.

[58] Salhi, A.; Tighadouini, S.; El-Massaoudi, M.; Elbelghiti, M.; Bouyanzer, A.; Radi, S.; El Barkany, S.; Bentiss, F.; Zarrouk, A., Keto-enol heterocycles as new compounds of corrosion inhibitors for carbon steel in 1 M HCl: Weight loss, electrochemical and quantum chemical investigation, *J. Mol. Liq.* **2017**, *248*, 340-349, DOI: 10.1016/j.molliq.2017.10.040.

[59] El Faydy, M.; About, H.; Benhiba, F.; Lakhrissi, B.; Guenbour, A.; Bentiss, F.; Warad, I.; Ebenso, E. E.; Zarrouk, A., The inhibitory effect of two 5-alkylthio-8-hydroxyquinoline salts on steel C22E in a molar electrolyte of hydrochloric acid: Experimental and theoretical studies, *Surf. Interface.* **2020**, *20*, 100575, DOI: 10.1016/j.surfin.2020.100575.

[60] Mobin, M.; Parveen, M.; Aslam, R., Effect of different additives, temperature, and immersion time on the inhibition behavior of L-valine for mild steel corrosion in 5% HCl solution. *J. Phys. Chem. Solids.* **2022**, *161*, 110422, DOI: 10.1016/j.jpcs.2021.110422.

[61] About, H.; El Faydy, M.; Benhiba, F.; Rouifi, Z.; Boudalia, M.; Guenbour, A.; Zarrok, H.; Lakhrissi, B.; Oudda, H.; Warad, I.; Zarrouk, A., Synthesis, Experimental and Theoretical Investigation of Tetrazole Derivative as an Effective Corrosion Inhibitor for Mild Steel in 1 M HCl. *J. Bio- Tribo-Corros.* **2019**, *5*, 1-15, DOI: 10.1007/s40735-019-0233-9.

[62] Kellal, R., Benmessaoud Left, D.; Azzi, M.; Zertoubi, M., Insight on the corrosion inhibition performance of Glebionis coronaria plant extract in various acidic mediums, *J. Appl. Electrochem.* **2023**, *53*, 811-832, DOI: 10.1007/s10800-022-01813-8.

[63] El Faydy, M.; Benhiba, F.; Warad, I.; Saoiabi, S.; Alharbi, A.; Alluhaybi, A. A.; Lakhrissi, B.; Abdallah, M.; Zarrouk, A., Bisquinoline analogs as corrosion inhibitors for carbon steel in acidic electrolyte: Experimental, DFT, and molecular dynamics simulation approaches. *J. Mol. Struct.* **2022**, *1265*, 133389, DOI: 10.1016/J.MOLSTRUC.2022.133389.

[64] Mourya, P.; Singh, P.; Tewari, A. K.; Rastogi R. B.; Singh, M. M., Relationship between structure and inhibition behaviour of quinolinium salts for mild steel corrosion: Experimental and theoretical approach, *Corros. Sci.* **2015**, *95*, 71-87, DOI: 10.1016/j.corsci.2015.02.034.

[65] Abboud, Y.; Abourriche, A.; Saffaj, T.; Berrada, M.; Charrouf, M.; Bennamara, A.; Al Himidi, N.; Hannache, H., 2,3-Quinoxalinedione as a novel corrosion inhibitor for mild steel in 1 M HCl, *Mater. Chem. Phys.* **2007**, *105* (1), 1-5, DOI: 10.1016/j.matchemphys.2007.03.

[66] Kumar, U. P.; Albrakaty, R. H.; Wazzan, N.; Obot, I. B.; Safi, Z. S.; Shanmugan, S.; Liang, T., Insight into the nature of the ionic interactions between some aldehydes and Ni-W alloy: A theoretical study, *Mater. Today Commun.* **2020**, *22*, DOI: 10.1016/j.mtcomm.2019.100693.

[67] El Faydy, M.; Benhiba, F.; About, H.; Kerroum, Y.; Guenbour, A.; Lakhrissi, B.; Warad, I.; Verma, C.; Sherif, El-S. M.; Ebenso, E. E.; Zarrouk, A., Experimental and computational investigations on the anti-corrosive and adsorption behavior of 7-N,N'-dialkyaminomethyl-8-Hydroxyquinolines on C40E steel surface in acidic medium. *J. Colloid Interface Sci.* **2020**, *576*, 330–344, DOI: 10.1016/j.jcis.2020.05.010.

[68] Kharbach, Y.; Qachchachi, F. Z.; Haoudi, A.; Tourabi, M.; Zarrouk, A.; Jama, C.; Olasunkanmi, L. O.; Ebenso, E. E.; Bentiss, F., Anticorrosion performance of three newly synthesized isatin derivatives on carbon steel in hydrochloric acid pickling environment: Electrochemical. surface and theoretical studies. *J. Mol. Liq.,* **2017**, *246*, 302-316, DOI: 10.1016/j.molliq.2017.09.057.

[69] Benhiba, F.; Hsissou, R.; Abderrahim, K.; Serrar, H.; Rouifi, Z.; Boukhris, S.; Kaichouh, G.; Bellaouchou, A.; Guenbour, A.; Oudda, H.; Warad, I.; Zarrouk, A., Development of New Pyrimidine Derivative Inhibitor for Mild Steel Corrosion in Acid Medium, *Journal of Bio- and Tribo-Corrosion*, **2022**, *8* (2), 36, DOI: 10.1007/s40735-022-00637-5.

[70] El yaktini, A.; Lachiri.; El Faydy, M.; Benhiba, F.; Zarrok, H.; El Azzouzi, M.; Zertoubi, M.; Azzi, M.; Lakhrissi B.; Zarrouk, A., Inhibitor effect of new azomethine derivative containing an 8-hydroxyquinoline moiety on corrosion behavior of mild carbon steel in acidic media. *Int. J. Corros. Scale Inhib.* **2017**, *7* (4), 609-632, DOI: 10.17675/2305-6894-2018-7-4-9.

[71] Benhiba, F.; Sebbar, N. K.; Bourazmi, H.; Belghiti, M. E.; Hsissou, R.; Hökelek, T.; Bellaouchou, A.; Guenbour, A.; Warad, I.; Oudda, H.; Zarrouk, A.; Essassi, E. M., Corrosion inhibition performance of 4-(prop-2-ynyl)-[1,4]-benzothiazin-3-one against mild steel in 1M HCl solution: Experimental and theoretical studies, *Int. J. Hydrogen Energy*, **2021**, *465* (51), 25800-25818, DOI: 10.1016/j.ijhydene.2021.05.091.

[72] Mehmeti, V.; Podvorica, F. I.; Experimental and theoretical studies on corrosion inhibition of niobium and tantalum surfaces by Carboxylated graphene oxide, *Materials*, **2018**, *11*, 893, DOI: 10.3390/ma11060893.

[73] Charati, S. G.; Stern, S. A., Diffusion of Gases in Silicone Polymers: Molecular Dynamics Simulations, *Macromolecules*. **1998**, *31*, 5529-5535, DOI: 10.1021/ma980387e.